

Published in final edited form as:

Nat Chem. 2018 November ; 10(11): 1118–1125. doi:10.1038/s41557-018-0127-3.

## A Fluorescent Membrane Tension Probe

Adai Colom<sup>1,2,3</sup>, Emmanuel Derivery<sup>1,2,3,#</sup>, Saeideh Soleimanpour<sup>2,3</sup>, Caterina Tomba<sup>1,3</sup>, Marta Dal Molin<sup>2,3</sup>, Naomi Sakai<sup>2,3</sup>, Marcos González-Gaitán<sup>1,2,3</sup>, Stefan Matile<sup>2,3</sup>, and Aurélien Roux<sup>1,2,3,\*</sup>

<sup>1</sup>Biochemistry Department, University of Geneva, CH-1211 Geneva, Switzerland <sup>2</sup>Swiss National Centre for Competence in Research Programme Chemical Biology, CH-1211 Geneva, Switzerland <sup>3</sup>School of Chemistry and Biochemistry, University of Geneva, CH-1211 Geneva, Switzerland

### Abstract

Cells and organelles are delimited by lipid bilayers in which high deformability is essential to many cell processes such as motility, endocytosis and cell division. Membrane tension is therefore a major regulator of cell processes that remodel membranes, albeit one that is very hard to measure *in vivo*. Here we show that a planarizable push-pull fluorescent probe called FliptR (Fluorescent LIPid Tension Reporter) can monitor changes of membrane tension by changing its fluorescence lifetime as a function of the twist between its fluorescent groups. The fluorescence lifetime depends linearly on membrane tension within cells, enabling an easy quantification of membrane tension by fluorescence lifetime imaging microscopy (FLIM). We further show using model membranes that this linear dependency between lifetime of the probe and membrane tension relies on a membrane-tension dependent lipid phase separation. We also provide calibration curves that enable accurate measurement of membrane tension using FLIM.

---

Cells and organelles are delimited by lipid membranes. Membranes are fluid surfaces of approximately four nanometer thickness, and are diffusion barriers to most solutes, but not to water. Membrane shape changes can cause bending, shearing and stretching. In particular, membrane tension is defined as the derivative of the membrane free energy with area change<sup>1, 2</sup>. Lipid membranes are very resistant to stretch, supporting tensions up to 10<sup>-2</sup> N/m before lysis, with few percent of area change<sup>3, 4</sup>.

Membrane tension plays an essential role in numerous cell processes. At the whole cell level, membrane tension is tightly regulated during cell migration<sup>5, 6, 7, 8</sup>, cell spreading

---

Users may view, print, copy, and download text and data-mine the content in such documents, for the purposes of academic research, subject always to the full Conditions of use:[http://www.nature.com/authors/editorial\\_policies/license.html#terms](http://www.nature.com/authors/editorial_policies/license.html#terms)

\*correspondence to Aurelien.Roux@unige.ch.

#present address: MRC Laboratory of Molecular Biology, Francis Crick Avenue, Cambridge Biomedical Campus, Cambridge, CB2 0QH, UK

#### DATA availability statement.

The data sets generated during the current study are available from the corresponding author upon reasonable request.

#### Competing Interests.

The authors declare no competing financial and non-financial interest.

and phagocytosis<sup>9, 10</sup>. During cell division, membrane tension causes a volume instability between daughter cells that is counteracted by contraction of the actin cortex<sup>11</sup>. Increased tension delays the last step of cell division called abscission<sup>12</sup>. Membrane tension also regulates subcellular processes. For example, increased tension inhibits endocytosis<sup>13</sup> by counteracting clathrin polymerization<sup>14</sup> and activating membrane fission<sup>15</sup>. Membrane tension regulates the opening of mechanosensitive ion channels<sup>16</sup>, and the activity of TORC2, a major regulator of cell metabolism<sup>17</sup>. As a consequence of its multiple roles, membrane tension is constantly regulated by the cell<sup>18</sup>.

Despite its importance in the regulation of many cell processes, membrane tension remains notoriously difficult to measure in cells: so far, the only technique available is extraction of small membrane tubes from the plasma membrane<sup>5, 18, 19</sup>. Although this technique provided valuable insights over the past decade, it suffers from several limitations. First, the tube radius and the force required to maintain the tube – measurements necessary for the calculation of the tension – are complex to obtain independently<sup>5</sup>. Second, since the formation of the tube requires peeling the membrane off the actin cortex, the adhesion energy of the membrane onto the actin cortex adds up to the membrane tension value. Finally, this technique cannot measure tension of intracellular membranes such as organelles.

The importance of membrane tension in biological processes called for non-invasive fluorescent probes that would allow for its measurement in living cells. However, no existing tension probes was shown to be reliable in living cells<sup>20, 21, 22, 23, 24, 25, 26, 27, 28, 29, 30</sup>. One approach, technically challenging, is to use homo-FRET signal of mechanosensitive ion channels<sup>16</sup>. Among different mechanisms explored, Photoinduced electron Transfer (PeT) is better for voltage sensitivity<sup>26</sup>, whereas solvatochromism<sup>21, 28</sup> and excited-state deplanarization in molecular rotors<sup>23, 24, 28, 29, 30, 31</sup> are most promising for imaging membrane order.

Recently, we introduced the complementary ground-state planarization as a new approach to mechanosensitive membrane probes<sup>32</sup>. Planarizable push-pull probes can report lipid-packing changes through changes of their fluorescence parameters. Lipid packing is defined as the density of lipid acyl chains: higher lipid packing is reflected by tighter and more ordered acyl chains, whereas lower lipid packing corresponds to more spaced and disordered acyl chains. Thus, liquid-ordered phases have higher lipid packing than liquid-disordered phases. We showed that these planarizable push-pull probes can distinguish different phases with different order<sup>33</sup>. In more ordered phases, lipid packing is higher, as acyl chains applied a higher pressure that planarized the push-pulled probes.

Membrane tension is also expected to change lipid packing by stretching the lipids away. However, the area increase through stretch is very small, with a maximum of 8% before lysis<sup>34</sup>. Because our push-pull probes are extremely sensitive to lipid-packing, we wondered if they could nevertheless report changes of membrane tension. Among the several push-pull probes we designed<sup>2, 32, 33, 35, 36</sup>, we called the most promising probe for measuring membrane tension, **FliptR** (for Fluorescent LIPid Tension Reporter, Fig. 1a)<sup>2</sup>.

**FliptR** consists of two large dithienothiophene (DTT) “flippers”<sup>33</sup> (Fig. 1a). In a non-confining environment, the two flippers are twisted out of conjugation by repulsion between the methyls and the endocyclic sulfurs next to the connecting, rotatable bond. The negatively charged carboxylate in the headgroup<sup>2</sup> helps to assure oriented insertion into membranes. **FliptR** has high photostability<sup>2</sup>, partition almost equally into different membrane phase<sup>33</sup>, different fluorescence absorption/emission spectra between lipid phase<sup>2</sup>, do not change position upon lipid phase transition<sup>33</sup>, and do not disturb membrane order like, e.g. cholesterol<sup>36</sup>. **FliptR** can planarize upon increase of lateral pressure (Fig. 1b). Here, we report that **FliptR** can image a combination of lipid composition and membrane tension in live cells and artificial membranes.

## Results & Discussion

### FliptR reports lipid order in artificial membranes

With the aim of imaging membrane tension in living cells, the large change of **FliptR** fluorescence lifetime with lipid phase caught our interest, as it reflected a high sensitivity to lipid packing. Moreover, lifetime is independent of intensity, which changes by a factor 10 in the planarized state vs the twisted state and is thus also independent of the optical set-up used to measure it.

We first studied if fluorescence lifetime of the probe could report the ordering state of various lipid phases. We electroformed giant unilamellar vesicles (GUVs) of different compositions with 1 mol% **FliptR**, and we imaged their lifetime using Fluorescence Lifetime Imaging Microscopy (FLIM). Fluorescence emission decay curves were fitted with double exponentials from which two lifetimes  $\tau_1$  and  $\tau_2$  and two intensities  $I_1$  and  $I_2$  can be extracted (see methods). As in the case of **FliptR**, the second component of the lifetime,  $\tau_2$ , only accounts for a minority of the signal, with a low amount of photons  $I_2$  (Supplementary Fig. 1a). Lifetime data presented in the following correspond to the longest component,  $\tau_1$ . This is further justified by the fact that  $\tau_2$  values are more subjected to errors, as they are smaller and account for less events, and that since  $\tau_1$  is linked to the time taken for intramolecular charge transfer, it thus reports directly onto the mechanism by which **FliptR** senses applied forces.

The lifetime of **FliptR** increased with the proportion of lipids forming liquid-ordered ( $L_o$ ) phase: **FliptR** fluorescence lifetime was  $3.75 \pm 0.08$  ns (mean  $\pm$  SD, as in the rest of the text, unless noted.  $N = 11$ ,  $R=43$  Fig. 1c) for GUVs made only of DOPC which forms liquid-disordered phase ( $L_d$ ) above 0 °C,  $5.31 \pm 0.12$  ns ( $N = 5$ ,  $R=15$ ) for GUVs made of DOPC and cholesterol (DOPC:CL, 60:40) which increases lipid order and  $6.39 \pm 0.09$  ns ( $N = 5$ ,  $R=25$ ) for GUVs composed of brain sphingomyelin (SM) and CL (70:30), forming a liquid-ordered phase ( $L_o$ ). Moreover, when phase-separated GUVs were formed (DOPC:SM:CL 25:58:17), different domains could easily be imaged by measuring **FliptR** lifetime (Fig. 1c,  $L_d$  and  $L_o$ ). Interestingly, the lifetime of **FliptR** in one of the domains was close to that in DOPC:CL 60:40 membranes ( $4.79 \pm 0.21$  ns ( $N = 4$ ,  $R=5$ ), compared to 5.31 ns for DOPC:CL 60:40), while the lifetime in the other domain was very close to the one of GUVs made of SM and CL only ( $6.57 \pm 0.29$  ns ( $N = 4$ ,  $R=5$ )) compared to 6.39 ns for SM:CL

70:30). These results show that **FliptR** is sensitive to lipid composition by detecting the various packing of lipids in different phases with different order (Fig. 1c)2.

### FliptR reports lipid order in cellular membranes

We then tested if **FliptR** could detect lipid composition and/or phase differences in living cells. We used HeLa fibroblastic cells and MDCK epithelial cells, and when micromolar amounts of **FliptR** were added to the medium of non-confluent HeLa and MDCK cells, plasma membrane staining appeared in less than one minute, with enough signal to measure the lifetime accurately (Fig. 2a, Supplementary Video 1). However, in epithelial cells, the apical membrane has been reported to form a large  $L_o$  domain due to the enrichment in shingolipids and cholesterol, while the basolateral membrane is reported to form a less ordered lipid phase<sup>37</sup>, in which **FliptR** required more time to reach the basolateral side (Supplementary Fig. 1b). This may be due to the diffusion barrier created by the tight junctions between the apical side (to which **FliptR** is delivered) and the basolateral side. **FliptR** stably remained in the plasma membrane, even though a limited endosomal labeling appeared after two hours of incubation with **FliptR**, most probably due to endocytic recycling of the probe (Supplementary Fig. 1b). We did not notice any cell growth and/or viability defects up to four days of culture in the presence of **FliptR** (Supplementary Fig. 1b).

In polarized confluent MDCK cells grown on microstructured surfaces in order to provide different orientations of the cells towards the microscope, two clearly different lifetimes were observed (Fig. 2b). Lifetime on the apical side (towards the medium) is higher than on the basolateral (Fig. 2b, red color on the apical and green on the basolateral), matching with the lipid order difference in these two parts of the cells<sup>37, 38</sup>. This finding clearly showed that **FliptR** also detects lipid packing differences in different parts and/or compartments of epithelial cells.

### FliptR reports changes of osmotic pressure

We then wondered if **FliptR** could detect changes in membrane tension in cells. A common way to change membrane tension of cells is to apply osmotic shocks: during hypoosmotic shocks (low osmotic pressure  $\Pi$  from the cell culture media), cell volume and plasma membrane tension increase<sup>39, 40</sup>. On the contrary, under hyperosmotic shock (high osmolarity  $\Pi$ ), volume and membrane tension decrease (Fig. 3a)<sup>40, 41</sup>. When applying hypoosmotic shocks ( $\Pi < 0.3$  Osm) on HeLa and MDCK cells loaded with **FliptR**, we robustly observed longer lifetimes than in isoosmotic conditions ( $\Pi = 0.3$  Osm), while being shorter under hyperosmotic shocks ( $\Pi > 0.3$  Osm) (Fig. 3b). Whereas **FliptR** fluorescence lifetime  $\tau_1$  stayed constant when cells were kept in isoosmotic conditions (Supplementary Fig. 2a), it rapidly changed after hypoosmotic and hyperosmotic shocks (Supplementary Fig. 2b). Overall, the dependence of  $\tau_1$  to osmotic pressure  $\Pi$  from the cell media was linear for both HeLa and MDCK cells (Fig. 3b), but the slopes were clearly different (slope =  $-0.52 \pm 0.03$  vs  $-0.84 \pm 0.04$  ns·Osm<sup>-1</sup>, respectively, mean  $\pm$  SE). Moreover, a better fit was obtained by fitting hypoosmotic data independently of hyperosmotic data (see Supplementary Fig. 2c). In this case, both for HeLa and MDCK, slopes of hypoosmotic data are about 0.3-0.4 ns·Osm<sup>-1</sup> less than hyperosmotic data (HeLa: Hypo,  $-0.27 \pm 0.13$  ns·Osm<sup>-1</sup>

and Hyper:  $-0.59 \pm 0.04 \text{ ns}\cdot\text{Osm}^{-1}$ ; MDCK: Hypo,  $-0.50 \pm 0.33 \text{ ns}\cdot\text{Osm}^{-1}$ , Hyper:  $-0.88 \pm 0.07 \text{ ns}\cdot\text{Osm}^{-1}$ , mean  $\pm$  SE). This may be explained by lowering of lipid packing upon tension increase (see below).

To test the possibility that membrane-tension dependent changes of the **FliptR** lifetime were not coupled to cell active processes such as cortical acto-myosin contraction or active ion pumping, osmotic shocks were applied to GUVs with a lipid composition mimicking the cell plasma membrane (POPC:SM:CL 57:14:29) and loaded with **FliptR** (Fig. 3a). We found that **FliptR** lifetime  $\tau_1$  also increased with hypoosmotic shocks, and decreased with hyperosmotic shocks, in a similar way than in cells (Fig. 3b). Similarly, **FliptR** lifetime changed linearly with  $\Pi$ , even though changes were smaller (slope =  $-0.22 \text{ ns}\cdot\text{Osm}^{-1}$ ). The robust change of  $\tau_1$  proportionally to  $\Pi$  suggested that the lifetime of **FliptR** could monitor changes of plasma membrane tension.

### FliptR reports membrane tension in cells

To measure membrane tension while applying osmotic shocks to the same cell, optical tweezers were used to pull away concanavalin A-coated polystyrene beads previously attached to the cell membrane and produce thin membrane tubes (Fig. 3c)<sup>42</sup>. The force required to hold the bead is a direct measure – although not absolute – of cell membrane tension. We calculated the membrane tension  $\sigma$  from the force data using measured value of the cell membrane bending rigidity, typically  $0.14 \text{ pN}\cdot\mu\text{m}$ , corresponding to  $35 \text{ k}_B T$ .

We then applied an osmotic shock by flushing a new solution in the microscopy chamber (see methods) while recording **FliptR** lifetime and the tube force. Hypoosmotic shocks led to a moderated increase of the tube force, indicating a slight increase of membrane tension, whereas hyperosmotic shocks led to a dwindle of the tube force, indicating a large membrane tension drop (Fig. 3d). The change of  $\tau_1$  was linear with membrane tension  $\sigma$ , increasing with increasing tension. For MDCK cells, the slope was  $2.38 \pm 0.18 \text{ ns}\cdot\text{m}\cdot\text{mN}^{-1}$ , until reaching saturation for tension values above  $0.6 \text{ mN}\cdot\text{m}^{-1}$ , and  $0.196 \pm 0.07 \text{ ns}\cdot\text{m}\cdot\text{mN}^{-1}$  after this limit (Fig. 3d). For HeLa cell, the dependence was similar, from 0 to  $0.6 \text{ mN}\cdot\text{m}^{-1}$  the slope was  $0.78 \pm 14 \text{ ns}\cdot\text{m}\cdot\text{mN}^{-1}$ , and  $0.26 \pm 0.06 \text{ ns}\cdot\text{m}\cdot\text{mN}^{-1}$  on higher tensions (Fig. 3d). Importantly, the change of slope (Fig. 3d) happens for membrane tension values obtained in isoosmotic conditions. Values higher than the value of membrane tension in isotonic conditions were obtained for hypoosmotic shocks, whereas membrane tension values below the isotonic conditions were obtained with hypertonic shock. Thus, the change of slope happening at isotonic conditions may be due to an additional effect acting on **FliptR** in the hypotonic conditions. As for lifetime as a function of osmotic pressure (Fig. 3b), this additional effect may be reduction of lipid-packing (see below). These results clearly showed that **FliptR** fluorescence lifetime reports membrane tension in cells, and that calibration is needed for each cell type.

### The **FliptR** response in single lipid phase membrane is inverse than in cells

The response of mechanosensitive flipper probe **FliptR** to changes of membrane tension in cells and GUVs (Fig. 3) could conceivably originate from several structural changes (Fig. 4). A change in lipid packing is perhaps the most intuitive outcome of membrane tension (Fig.

4a,b)4, 34, 43. However, increasing distances between lipid acyl chains upon membrane tension increase should result in a more deplanarized state of **FliptR**. Increasing tension should thus lead to decreasing lifetimes, the opposite response to the one observed in cells (Fig. 3).

We nevertheless went on testing this hypothesis using SM:CL 70:30 GUVs which consist of  $L_o$  phase, thus with high lipid packing at low membrane tension, reflected by the high **FliptR** lifetime values in those membranes (Fig. 1c). By aspirating these  $L_o$  GUVs labeled with 1 mol% **FliptR** with a micropipette, we control and change their tension. Their tension was measured by the extraction of a small membrane tubes with optical tweezers (Fig. 5a,b). As expected from our hypothesis,  $L_o$  SM:CL 70:30 GUVs revealed a linear decrease in **FliptR** lifetime with increasing tension with a slope =  $-1.32 \pm 0.19$  ns·m·mN<sup>-1</sup> (Fig. 5b). Thus indeed, in single-phased membranes, **FliptR** response to tension is dominated by loosened lipid packing with increasing distances between lipid tails (Fig. 4b). This effect could also be seen as a tension-induced lipid phase transition: tension may exert pulling forces onto the acyl chains of lipids, allowing them to melt from  $L_o$  into  $L_d$  phase.

In membranes with a composition closer to plasma membrane, i.e., POPC:SM:CL 57:14:29, the decrease in **FliptR** lifetime in response to increasing tension was much less pronounced (Fig. 5b, slope =  $-0.27 \pm 0.05$  ns·m·mN<sup>-1</sup>). Because of the pipette aspiration used in these experiments, only conditions where membrane tension increased could be tested (Fig. 3b). It suggested that even if the response of these GUVs to micropipette aspiration is dominated by loosened lipid packing, another molecular mechanism would lower the response of **FliptR** to increasing tension. Indeed, the small decrease in **FliptR** lifetime with increasing tension applied by micropipette aspiration (Fig. 5b) was contrary to the significant increase in **FliptR** lifetime with decreasing osmotic pressure (membrane tension increase) in cells and GUVs (Fig. 3b).

### The **FliptR** response to tension depends on lipid phase separation

We then studied the nature of this additional molecular mechanism. One of the possible explanations for the increasing **FliptR** lifetime with increasing tension is that lipid tails would tilt upon increase of surface area (Fig. 4c). Tilted lipid tails could be a way to adapt the rapid change of surface as observed in stretched polymer chemistry<sup>44</sup>. Also, tilted lipid tails are a characteristic feature of peculiar gel phases called  $L_{\beta}$ , to accommodate tight packing with surface increase<sup>45</sup>. Chain stretching and lipid tilting in response to increasing membrane tension would cause lateral compression of the acyl chains, leading to **FliptR** planarization and increasing its lifetime. This effect is expected to be independent of the lipid phase. We thus tested this tilting hypothesis in pure  $L_d$  GUVs composed of DOPC only, and subjected to hypo- or hyperosmotic shocks, which did not change the lifetime of **FliptR** (Supplementary Fig. 3a). We thus concluded that the tilting was not the mechanism causing lifetime changes in response to tension changes in cells.

Planarizable push-pull probes have been suspected early on to be planarizable also by voltage because of macrodipole-potential interactions<sup>32</sup>. Cell membranes have a voltage potential, created by ionic gradients across them. Although experimental support for

significant voltage sensitivity could not be obtained so far, possible contributions to the response of **FliptR** probe to tension had to be tested. For this purpose, we loaded neurons – which are cells with high membrane potential – with **FliptR** and depolarized them with an isoosmotic buffer containing 47 mM of KCl (see Methods). During the KCl treatment, **FliptR** lifetime did not change significantly (Supplementary Fig. 4). However, upon addition of a 700 mOsm hyperosmotic sucrose solution, **FliptR** lifetime dropped significantly (Supplementary Fig. 4). We thus concluded that **FliptR** was insensitive to membrane polarization.

The last possibility to explain the coupled changes of lifetime and tension was that tension changes would induce phase separation (Fig. 4d). Recent studies have shown that changes of tension can cause a lipid phase separation to accommodate the area change<sup>46, 47, 48, 49, 50, 51</sup>. In this case, while the membrane is initially homogeneous, domains appear upon increase of membrane tension. The newly formed  $L_d$  phase supports most of the stretch, while  $L_o$  domains cluster the lipids that cannot be stretched easily. To test this possibility, GUVs were prepared with a lipid composition (DOPC:SM:CL 1:1:1) that mimics the phase separation state of cell membranes by being close to the transition from  $L_d$  to mixed  $L_d$ - $L_o$  phases<sup>52</sup> – thus more prone to phase separate upon tension. These GUVs were aspirated into a micropipette to increase their tension (Fig. 5a). As expected, the formation of large domains (visualized through the lifetime image of **FliptR**, see also Fig. 1c) could reproducibly be observed in GUVs aspirated in micropipettes after an abrupt increase of aspiration (Fig. 5c). Moreover, upon aspiration, while the lifetime increased in the  $L_o$  domains and decreased in the  $L_d$  domains, the average lifetime of **FliptR** on the entire GUV increased upon aspiration (see Fig. 5c, middle and right panels). This shows that the **FliptR** lifetime increase upon membrane tension increase in cells (Fig. 3d) can be attributed to increased lipid phase separation. To further support this hypothesis, we directly investigated changes in the homogeneity of the membrane **FliptR** lifetime upon hypertonic shocks. At rest, the **FliptR** lifetime image showed areas of higher life time (see Fig. 5d and suppl. video 2), which are probably related to inhomogeneities of the lipid composition. After a hypertonic shock, these areas seemed to disappear (see Fig. 5d and suppl. video 2), suggesting that upon membrane tension decrease, the local plasma membrane composition becomes more homogeneous.

Thus, **FliptR** response to tension in cells strongly depends on tension-induced change in phase separation, a mechanism that explains the overall change of **FliptR** lifetime upon osmotic shocks in cells. Upon tension-induced phase separation, the overall lifetime response is dominated by **FliptR** in the more-ordered phase (Fig. 4a,d). This explanation seems reasonable considering the almost equal partitioning of **FliptR** in  $L_d$  and  $L_o$  phases<sup>33</sup>, but larger area of  $L_o$  phase compared to  $L_d$  resulting from tension-induced phase separation (Fig. 5c)<sup>46, 47</sup>. Moreover, the absorptivity of **FliptR** probe in  $L_o$  phase is higher than in  $L_d$  phase at the excitation wavelength (485 nm)<sup>53</sup>. Thus, the contribution to the overall lifetime counts in FLIM histograms from **FliptR** molecules in  $L_o$  phase is larger than from those in  $L_d$  phase, as seen from the increased photon counts when phase separated (Fig. 5c). Similarly, decreasing **FliptR** lifetime by decreasing tension under hyperosmotic stress is

explained by reduction of the phase separation, most probably because of partial mixing of the  $L_o$ - $L_d$  phases<sup>48, 49</sup>.

## Conclusion

We report here the use of **FliptR** as a fluorescent probe that allows reliable imaging of membrane tension in living cells and model membranes by FLIM. The intrinsic dependence of **FliptR** response on lipid composition naturally prevents the attribution of absolute values of **FliptR** lifetime to membrane tension that would be valid for all cells. We provide here calibration curves available to other users for two of the most commonly used cell lines, MDCK and HeLa cells (Fig. 3d).

Increasing lifetimes with increasing tension shows that **FliptR** planarizes upon tension increase. This response is consistent with tension-induced lipid phase separation into more ordered domains with more planarized probes and less ordered domains with more deplanarized probes. These tension-induced domains have been observed previously in model membranes with other techniques<sup>46, 47, 48, 49, 50, 51</sup>. In cells, the size of the tension-induced microdomains is probably below detection limits and they might move too fast for FLIM imaging. Even then, the observed overall increase in lifetime with increased membrane tension is consistent with the tension-induced domain formation as in GUVs.

**FliptR** deplanarization due to lowering of lipid packing by tension is observed in ordered membrane phases that do not phase separate in our experimental conditions. The typical value of this response (Fig. 5b,  $-1.32$  to  $-0.27$  ns·m·mN<sup>-1</sup>) is in the range of the response due to phase separation (Fig. 3d,  $0.57$ - $2.38$  ns·m·mN<sup>-1</sup>). However, in cells the contribution of both effects may be very different in hypo and hyperosmotic conditions: in hypoosmotic conditions, the overall change of lifetime was fairly small, whereas dramatic changes of the lifetime were observed for hyperosmotic conditions (see Fig. 3b and 3d). This could be explained by the fact that in hypoosmotic shocks, both changes in lipid packing (see Figs. 4b and 5b) and phase separation (Figs. 4d and 5c) would contribute to change the lifetime. As both effects have opposite contributions, but of the same order of magnitude, they would annihilate, the overall response being negligible. In hyperosmotic conditions however, the lipids are relaxed to their most compressed state even for small hyperosmotic shocks. In this case, only changes of phase separation could thus act on **FliptR**, leading to larger changes of the lifetime with decreasing membrane tension (see Fig. 3d). Eventual contributions from lipid tilting and changes in transmembrane voltage to the response of **FliptR** to tension could be excluded.

**FliptR** offers an ideal combination of characteristics to accurately image membrane tension in live cells. It combines: i) partitioning into different membrane domains without strong preference<sup>33</sup>; ii) negligible disturbance of the structure of the surrounding membrane<sup>36</sup>; iii) specific labeling of the plasma membrane<sup>2</sup>; iv) negligible fluorescence in water<sup>2, 54, 55</sup> and v) insensitivity to membrane potential. An intrinsic limitation of **FliptR** is to report lipid packing, which depends on the combination of tension and lipid composition. However, it is difficult to imagine another way than sensing lipid packing to report membrane tension at the molecular level. Thus, the design of a membrane tension probe insensitive to lipid

composition is unlikely. Nevertheless, despite this limitation, **FliptR** accurately reports membrane tension changes, which are occurring on a time scale of a few seconds, easily discriminated from lipid composition changes that occur over tens of minutes.

It is safe to predict that **FliptR** will not remain the only tension probe to do so. Established systems to image changes in membrane order such as molecular rotors<sup>21, 23, 24, 25, 28, 29, 30</sup> or solvatochromic probes<sup>23, 55, 56</sup> could also function as tension probes. However, further development will be required to adapt these molecules to the list of characteristics required to measure membrane tension. For instance, sufficient partitioning into the  $L_o$  membranes is difficult to achieve<sup>21, 23, 24, 25, 28, 29, 30, 57</sup>, as these fluorescent probes disturb the local order of lipids. This study is proposed as an example to encourage fluorescent probe experts to elaborate on the compatibility of their systems with the imaging of membrane tension.

The availability of **FliptR** opens new opportunities to study cell membrane processes by offering the unique possibility to image directly membrane tension in living cells. We foresee new possibilities in studying the role of membrane tension during cell division, endocytosis or cell migration. Preliminary studies focusing on the activation of TORC2 signaling by membrane tension in yeast cells fully support these high expectations, including corroborative evidence for tension-induced phase separation<sup>58</sup>. Moreover, the future design of flipper probes localizing specifically to organelles will enable the community to study intracellular membrane tension, as well as its regulation. Finally, in tissue cells, membrane tension may be a direct reporter of force fields existing in growing tissues. Further studies will determine if the **FliptR** probe can prove itself a direct way to measure those force fields during development.

## Materials and Methods

### FliptR synthesis

FliptR probes were synthesized following reported procedures<sup>30</sup>. Analytical data of the final product were identical with the reported data and thus consistent with structure and purity of the mechanophore.

### Giant unilamellar vesicles preparation and lifetime imaging

Giant unilamellar vesicles (GUVs) were prepared by the electroformation technique. All lipids were purchased from Avanti Polar Lipids (Alabaster, USA). The lipid solutions used (2mg/ml) were (1) pure 1,2-dioleoyl-*sn*-glycero-3-phosphocholine (DOPC), a (2) mixture of DOPC 70 mol% and cholesterol 30 mol%, (3) N-(dodecanoyl)-sphing-4-enine-1-phosphocholine (Brain Sphingomyelin) 58 mol%, DOPC 25 mol%, cholesterol 17 mol%, (4) 70 mol% Brain Sphingomyelin and 30 mol% of cholesterol, and finally (5) 1-palmitoyl-2-oleoyl-*sn*-glycero-3-phosphocholine (POPC) 80 mol%, Sphingomyelin 18.97 mol% and cholesterol 40 mol%. Each lipid solution on  $\text{CHCl}_3$  was supplemented with **FliptR** (from DMSO solution) at 1% mol and 0.03% mol DSPE-PEG2000-Biotin.

The lipid solution was spread on ITO-coated glass slides, previously cleaned with bi-distilled water, EtOH and  $\text{CHCl}_3$ . The ITO-slides with the lipid was dried by keeping the

slides for 2 h at 30°C. The chamber was assembled using separated by O-ring, filled with a 297 mOsm sucrose solution and blocked with silicone elastomer. An electric field (10 Hz, 1.1 V) was then applied for 2 h at 55 °C in case of sphingomyelin-containing lipid mixes or at RT if not.

Lifetime imaging was made in a flow chamber described above for osmotic shocks on cells. Prior to addition of the GUVs solution, the coverslip was incubated with avidin (Avidin from egg white, Life Technologies, 434401) at 0.1mg/ml for 10 min. Avidin was washed out 3 times with ddH<sub>2</sub>O, and the flow chamber was filled with 200 µl of PBS. 5 µl of GUVs were then flushed in the flow chamber. Once the GUVs started to partially adhere to the surface and to avoid further adhesion, which could lead to GUV bursting, the remaining glass-bound avidin was blocked by flowing BSA-biotin (1 mg/ml, Sigma-Aldrich, A8549) during 15 minutes.

### Lifetime measurements

FLIM imaging was performed using a Nikon Eclipse Ti A1R microscope equipped with a Time Correlated Single-Photon Counting module from PicoQuant59. Excitation was performed using a pulsed 485nm laser (PicoQuant, LDH-D-C-485) operating at 20 MHz, and emission signal was collected through a bandpass 600/50nm filter using a gated PMA hybrid 40 detector and a TimeHarp 260 PICO board (PicoQuant). SymPhoTime 64 software (PicoQuant) was then used to fit fluorescence decay data (from full images or regions of interest) to a dual exponential model after deconvolution for the instrument response function (measured using the backscattered emission light of a 1µM fluorescein solution with 4M KI). Data was expressed as means ± standard deviation of the mean. The full width at half-maximum (FWHM) response of the instrument was measured at 176 ps.

Supplementary figure 1a shows all parameters extracted from the fits of **FlipTR** in various GUV compositions. As similar tendencies were seen for  $\tau_1$  and  $\tau_2$ , the longest lifetime ( $\tau_1$ ) obtained by the double exponential fits was used for all subsequent graphs.

### Optical Tweezers Tube Pulling Experiment

Tube pulling tension measurements were performed using a modified version of published setup<sup>15</sup>, which allows simultaneous bright-field and FLIM imaging on an inverted Nikon Eclipse Ti A1R microscope. A membrane nanotube was formed by pulling away a micropipette-aspirated GUV, whose membrane was attached to a streptavidin-coated bead (3.05 µm diameter, Spherotec, Lake Forest, Illinois, USA) held in a fixed optical trap. The trap was obtained by focusing an ytterbium fiber laser (IPG laser, Burbach, Germany) through a 100X 1.3 NA oil immersion objective (Nikon, Tokyo, Japan). Force measurements were made measuring the displacement of the bead in the optical trap via a C-MOS Camera (Pixelink, Ottawa, Canada) with a home-made video recorder and bead tracking software under Matlab. The force  $F$  exerted on the bead was calculated from the Hooke's law:  $F = k \cdot x$ , where  $k$  is the stiffness of the trap ( $k = 8.58 \text{ pN}\cdot\text{pix}^{-1} \cdot \text{W}^{-1}$ ) and  $x$  the displacement of the bead from its initial, zero force position.

## Data processing

Images were analyzed and processed with SymPho Time64 and ImageJ. All the graphs were made with GraphPad Prism 7. Blender software have been used for the drawings.

## Supplementary Material

Refer to Web version on PubMed Central for supplementary material.

## Acknowledgments

The authors would like to thank Vincent Mercier, Guillaume Molinard and Marine Laporte for technical support and useful scientific discussions. The authors thank the NMR, the MS and the Bioimaging platforms for services, and the University of Geneva, the Swiss National Centre of Competence in Research (NCCR) Chemical Biology, the NCCR Molecular Systems Engineering and the Swiss NSF for financial support. AR acknowledges funding from Human Frontier Science Program CDA-0061-08, the Swiss National Fund for Research Grants N°31003A\_130520, N°31003A\_149975 and N°31003A\_173087, and the European Research Council Starting Grant N° 311536 (2011 call). ED acknowledges funding from Human Frontier Science Program (LT00305/2011-L).

## References

1. Helfrich W. Elastic properties of lipid bilayers : theory and possible experiments. *Zur Naturforschung*. 1973; 28c:693–703.
2. Soleimanpour S, Colom A, Derivery E, Gonzalez-Gaitan M, Roux A, Sakai N, et al. Headgroup engineering in mechanosensitive membrane probes. *Chem Commun (Camb)*. 2016; 52(100):14450–14453. [PubMed: 27901525]
3. Evans E, Heinrich V, Ludwig F, Rawicz W. Dynamic tension spectroscopy and strength of biomembranes. *Biophys J*. 2003; 85(4):2342–2350. [PubMed: 14507698]
4. Rawicz W, Smith BA, McIntosh TJ, Simon SA, Evans E. Elasticity, strength, and water permeability of bilayers that contain raft microdomain-forming lipids. *Biophys J*. 2008; 94(12):4725–4736. [PubMed: 18339739]
5. Lieber AD, Schweitzer Y, Kozlov MM, Keren K. Front-to-rear membrane tension gradient in rapidly moving cells. *Biophys J*. 2015; 108(7):1599–1603. [PubMed: 25863051]
6. Lieber AD, Yehudai-Resheff S, Barnhart EL, Theriot JA, Keren K. Membrane tension in rapidly moving cells is determined by cytoskeletal forces. *Curr Biol*. 2013; 23(15):1409–1417. [PubMed: 23831292]
7. Pontes B, Monzo P, Gole L, Le Roux AL, Kosmalska AJ, Tam ZY, et al. Membrane tension controls adhesion positioning at the leading edge of cells. *J Cell Biol*. 2017
8. Gauthier NC, Masters TA, Sheetz MP. Mechanical feedback between membrane tension and dynamics. *Trends Cell Biol*. 2012; 22(10):527–535. [PubMed: 22921414]
9. Gauthier NC, Fardin MA, Roca-Cusachs P, Sheetz MP. Temporary increase in plasma membrane tension coordinates the activation of exocytosis and contraction during cell spreading. *Proc Natl Acad Sci U S A*. 2011; 108(35):14467–14472. [PubMed: 21808040]
10. Masters TA, Pontes B, Viasnoff V, Li Y, Gauthier NC. Plasma membrane tension orchestrates membrane trafficking, cytoskeletal remodeling, and biochemical signaling during phagocytosis. *Proc Natl Acad Sci U S A*. 2013; 110(29):11875–11880. [PubMed: 23821745]
11. Sedzinski J, Biro M, Oswald A, Tinevez JY, Salbreux G, Paluch E. Polar actomyosin contractility destabilizes the position of the cytokinetic furrow. *Nature*. 2011; 476(7361):462–466. [PubMed: 21822289]
12. Lafaurie-Janvore J, Maiuri P, Wang I, Pinot M, Manneville JB, Betz T, et al. ESCRT-III assembly and cytokinetic abscission are induced by tension release in the intercellular bridge. *Science*. 2013; 339(6127):1625–1629. [PubMed: 23539606]
13. Boulant S, Kural C, Zeeh JC, Ubelmann F, Kirchhausen T. Actin dynamics counteract membrane tension during clathrin-mediated endocytosis. *Nat Cell Biol*. 2011; 13(9):1124–1131. [PubMed: 21841790]

14. Saleem M, Morlot S, Hohendahl A, Manzi J, Lenz M, Roux A. A balance between membrane elasticity and polymerization energy sets the shape of spherical clathrin coats. *Nat Commun.* 2015; 6:6249.
15. Morlot S, Galli V, Klein M, Chiaruttini N, Manzi J, Humbert F, et al. Membrane shape at the edge of the dynamin helix sets location and duration of the fission reaction. *Cell.* 2012; 151(3):619–629. [PubMed: 23101629]
16. Wang Y, Liu Y, DeBerg HA, Nomura T, Hoffman MT, Rohde PR, et al. Single molecule FRET reveals pore size and opening mechanism of a mechano-sensitive ion channel. *eLife.* 2014; 3:e01834. [PubMed: 24550255]
17. Berchtold D, Piccolis M, Chiaruttini N, Riezman I, Riezman H, Roux A, et al. Plasma membrane stress induces relocalization of Slm proteins and activation of TORC2 to promote sphingolipid synthesis. *Nat Cell Biol.* 2012; 14(5):542–547. [PubMed: 22504275]
18. Sinha B, Koster D, Ruez R, Gonnord P, Bastiani M, Abankwa D, et al. Cells respond to mechanical stress by rapid disassembly of caveolae. *Cell.* 2011; 144(3):402–413. [PubMed: 21295700]
19. Gabella C, Bertseva E, Bottier C, Piacentini N, Bornert A, Jeney S, et al. Contact angle at the leading edge controls cell protrusion rate. *Curr Biol.* 2014; 24(10):1126–1132. [PubMed: 24794299]
20. Warshaviak DT, Muellner MJ, Chachisvilis M. Effect of membrane tension on the electric field and dipole potential of lipid bilayer membrane. *Biochim Biophys Acta (BBA) - Biomembranes.* 2011; 1808(10):2608–2617. [PubMed: 21722624]
21. Zhang Y-L, Frangos JA, Chachisvilis M. Laurdan fluorescence senses mechanical strain in the lipid bilayer membrane. *Biochem Biophys Res Commun.* 2006; 347(3):838–841. [PubMed: 16857174]
22. Templer RH, Castle SJ, Rachael Curran A, Rumbles G, Klug DR. Sensing isothermal changes in the lateral pressure in model membranes using di-pyrenyl phosphatidylcholine. *Faraday Discuss.* 1999; 111:41–53.
23. Haidekker MA, Theodorakis EA. Ratiometric mechanosensitive fluorescent dyes: Design and applications. *J mat chem C.* 2016; 4(14):2707–2718.
24. Kuimova MK, Botchway SW, Parker AW, Balaz M, Collins HA, Anderson HL, et al. Imaging intracellular viscosity of a single cell during photoinduced cell death. *Nat Chem.* 2009; 1:69. [PubMed: 21378803]
25. Vysniauskas A, Balaz M, Anderson HL, Kuimova MK. Dual mode quantitative imaging of microscopic viscosity using a conjugated porphyrin dimer. *Physical Chemistry Chemical Physics.* 2015; 17(11):7548–7554. [PubMed: 25706402]
26. Kulkarni RU, Miller EW. Voltage Imaging: Pitfalls and Potential. *Biochemistry.* 2017; 56(39):5171–5177. [PubMed: 28745864]
27. M'Baye G, Mély Y, Duportail G, Klymchenko AS. Liquid Ordered and Gel Phases of Lipid Bilayers: Fluorescent Probes Reveal Close Fluidity but Different Hydration. *Biophys J.* 95(3):1217–1225.
28. Klymchenko AS. Solvatochromic and Fluorogenic Dyes as Environment-Sensitive Probes: Design and Biological Applications. *Acc Chem Res.* 2017; 50(2):366–375. [PubMed: 28067047]
29. Su D, Teoh CL, Wang L, Liu X, Chang Y-T. Motion-induced change in emission (MICE) for developing fluorescent probes. *Chem Soc Rev.* 2017; 46(16):4833–4844. [PubMed: 28692081]
30. Sherin PS, López-Duarte I, Dent MR, Kubánková M, Vyšniauskas A, Bull JA, et al. Visualising the membrane viscosity of porcine eye lens cells using molecular rotors. *Chem Sci.* 2017; 8(5):3523–3528. [PubMed: 28580097]
31. Vyšniauskas A, Ding D, Qurashi M, Boczarow I, Balaz M, Anderson HL, et al. Tuning the Sensitivity of Fluorescent Porphyrin Dimers to Viscosity and Temperature. *Chem Eur J.* 2017; 23(46):11001–11010. [PubMed: 28480989]
32. Fin A, Vargas Jentsch A, Sakai N, Matile S. Oligothiophene amphiphiles as planarizable and polarizable fluorescent membrane probes. *Angew Chem Int Ed.* 2012; 51(51):12736–12739.
33. Dal Molin M, Verolet Q, Colom A, Letrun R, Derivery E, Gonzalez-Gaitan M, et al. Fluorescent flippers for mechanosensitive membrane probes. *J Am Chem Soc.* 2015; 137(2):568–571. [PubMed: 25584496]

34. Rawicz W, Olbrich KC, McIntosh T, Needham D, Evans E. Effect of chain length and unsaturation on elasticity of lipid bilayers. *Biophys J*. 2000; 79(1):328–339. [PubMed: 10866959]
35. Verolet Q, Dal Molin M, Colom A, Roux A, Guénee L, Sakai N, et al. Twisted Push-Pull Probes with Turn-On Sulfide Donors. *Helv Chim Acta*. 2017; 100(2):11564.
36. Neuhaus F, Zobi F, Brezesinski G, Molin MD, Matile S, Zumbuehl A. Correlation of surface pressure and hue of planarizable push-pull chromophores at the air/water interface. *Beilstein J Org Chem*. 2017; 13(1):1099–1105. [PubMed: 28684989]
37. Sampaio JL, Gerl MJ, Klose C, Ejsing CS, Beug H, Simons K, et al. Membrane lipidome of an epithelial cell line. *Proc Natl Acad Sci U S A*. 2011; 108(5):1903–1907. [PubMed: 21245337]
38. van Meer G, Simons K. Lipid polarity and sorting in epithelial cells. *J Cell Biochem*. 1988; 36(1): 51–58. [PubMed: 3277985]
39. Pietuch A, Brückner BR, Janshoff A. Membrane tension homeostasis of epithelial cells through surface area regulation in response to osmotic stress. *Biochim Biophys Acta*. 2013; 1833(3):712–722. [PubMed: 23178740]
40. Dai JW, Sheetz MP, Wan XD, Morris CE. Membrane tension in swelling and shrinking molluscan neurons. *J Neurosci*. 1998; 18(17):6681–6692. [PubMed: 9712640]
41. Alam Shibly SU, Ghatak C, Sayem Karal MA, Moniruzzaman M, Yamazaki M. Experimental Estimation of Membrane Tension Induced by Osmotic Pressure. *Biophys J*. 2016; 111(10):2190–2201. [PubMed: 27851942]
42. Gauthier NC, Rossier OM, Mathur A, Hone JC, Sheetz MP. Plasma membrane area increases with spread area by exocytosis of a GPI-anchored protein compartment. *Mol Biol Cell*. 2009; 20(14): 3261–3272. [PubMed: 19458190]
43. Ben-Shaul A. *Molecular Theory of Chain Packing, Elasticity and Lipid-Protein Interaction in Lipid Bilayers* Vol. 1. Elsevier; 1995. 359–401.
44. Mackley M. Stretching polymer chains. *Rheol Acta*. 2010; 49(5):443–458.
45. Koynova R, Caffrey M. Phases and phase transitions of the phosphatidylcholines. *Biochim Biophys Acta (BBA) - Reviews on Biomembranes*. 1998; 1376(1):91–145. [PubMed: 9666088]
46. Ho JCS, Rangamani P, Liedberg B, Parikh AN. Mixing Water, Transducing Energy, and Shaping Membranes: Autonomously Self-Regulating Giant Vesicles. *Langmuir*. 2016; 32(9):2151–2163. [PubMed: 26866787]
47. Ogl cka K, Rangamani P, Liedberg B, Kraut RS, Parikh AN. Oscillatory phase separation in giant lipid vesicles induced by transmembrane osmotic differentials. *eLife*. 2014; 3:e03695. [PubMed: 25318069]
48. Yanagisawa M, Imai M, Taniguchi T. Shape Deformation of Ternary Vesicles Coupled with Phase Separation. *Phys Rev Lett*. 2008; 100(14):148102. [PubMed: 18518074]
49. Ogl cka K, Sanborn J, Parikh AN, Kraut RS. Osmotic gradients induce bio-reminiscent morphological transformations in giant unilamellar vesicles. *Front Physiol*. 2012; 3:120. [PubMed: 22586404]
50. Chen D, Santore MM. Three dimensional (temperature-tension-composition) phase map of mixed DOPC-DPPC vesicles: Two solid phases and a fluid phase coexist on three intersecting planes. *Biochim Biophys Acta*. 2014; 1838(11):2788–2797. [PubMed: 25064155]
51. Hamada T, Kishimoto Y, Nagasaki T, Takagi M. Lateral phase separation in tense membranes. *Soft Matter*. 2011; 7(19):9061–9068.
52. Petruzielo RS, Heberle FA, Drazba P, Katsaras J, Feigenson GW. Phase behavior and domain size in sphingomyelin-containing lipid bilayers. *Biochim Biophys Acta*. 2013; 1828(4):1302–1313. [PubMed: 23337475]
53. Soleimanpour S, Colom A, Derivery E, Gonzalez-Gaitan M, Roux A, Sakai N, et al. Headgroup engineering in mechanosensitive membrane probes. *Chem Commun (Camb)*. 2016; 52(100): 14450–14453. [PubMed: 27901525]
54. Macchione M, Chuard N, Sakai N, Matile S. Planarizable Push–Pull Probes: Overtwisted Flipper Mechanophores. *ChemPlusChem*. 2017; 82(7):1062–1066.
55. Prifti E, Reymond L, Umebayashi M, Hovius R, Riezman H, Johnsson K. A Fluorogenic Probe for SNAP-Tagged Plasma Membrane Proteins Based on the Solvatochromic Molecule Nile Red. *ACS Chemical Biology*. 2014; 9(3):606–612. [PubMed: 24471525]

56. Mariana A, Francesco R, Martin H, Christian E, Erdinc S. Laurdan and Di-4-ANEPPDHQ probe different properties of the membrane. *J Phys D*. 2017; 50(13):134004.
57. Doval DA, Fin A, Takahashi-Umebayashi M, Riezman H, Roux A, Sakai N, et al. Amphiphilic dynamic NDI and PDI probes: imaging microdomains in giant unilamellar vesicles. *Org & Biomol Chem*. 2012; 10(30):6087–6093. [PubMed: 22499252]
58. Riggi M, Niewola-Staszewska K, Chiaruttini N, Colom A, Kusmider B, Soleimanpour S, Stahl M, Matile S, Roux A, Loewith R. A decrease in plasma membrane tension inhibits TORC2 activity via sequestration into PtdIns(4,5)P2-enriched domains. - Submitted, -(-): -
59. Wahl M, Koberling F, Patting M, Erdmann HR. Time-Resolved Confocal Fluorescence Imaging and Spectroscopy System with Single Molecule Sensitivity and Sub-Micrometer Resolution. *Curr Pharmaceut Biotech*. 2004; 5(3):299–308.

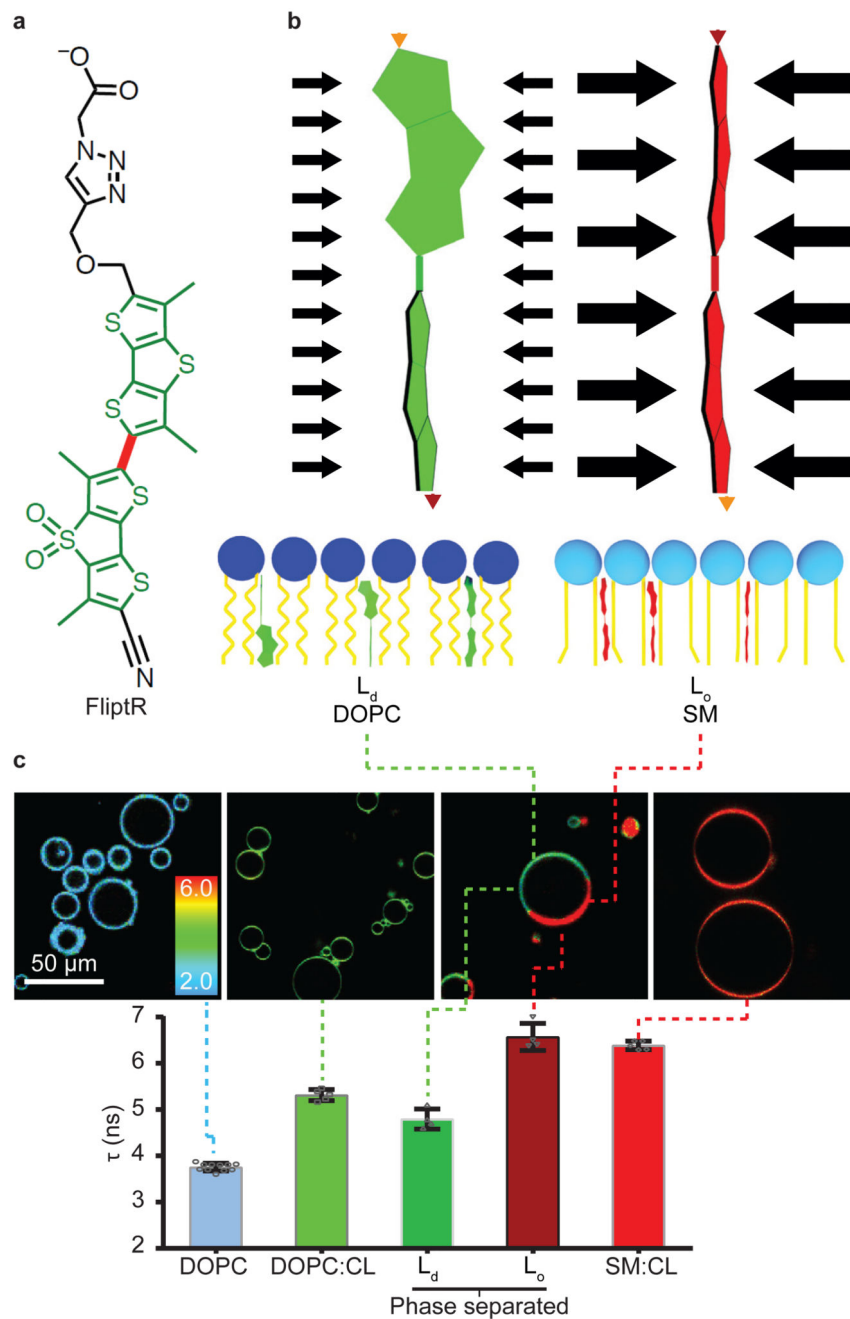


**Figure 1. The FliptR probe.**

(a) Chemical structure. The carbon bond around which the fluorescent groups (green) can twist is shown in red. (b) Pressure along the axis of the **FliptR** probe can planarize the two fluorescent groups, leading to changes in excitation maxima and fluorescence lifetime (see text). (c) Fluorescence lifetime  $\tau_1$  of **FliptR** as a function of lipid composition in GUVs, from liquid-disordered membrane ( $L_d$ ) to increasingly liquid-ordered membranes ( $L_o$ ). Compositions are: DOPC (N=5, R=15), DOPC:CL 60:40 (N=5, R=25), phase-separated DOPC:SM:CL 25:58:17 (N=4, R=5) and SM:CL 70:30 (N=5, R=25). Mean  $\pm$  SD.

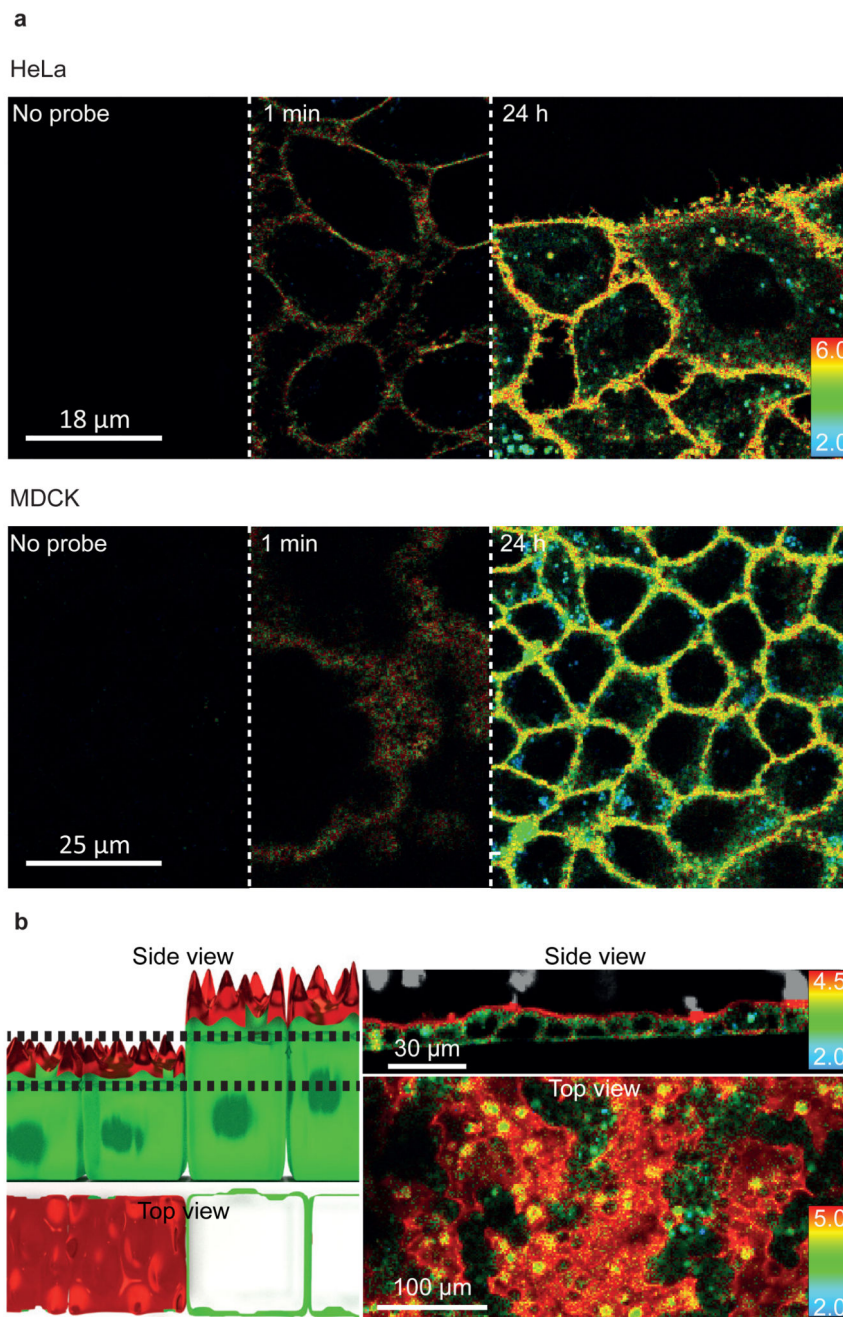


**Figure 2. Different FliptR lifetimes correspond to different lipid compositions in cells.** (a) Labelling of MDCK and HeLa cells with time. **FliptR** mostly stays in the plasma membrane. However, after 2h of incubation, bright spots with low lifetime values (i.e. more blue colors) are seen, probably corresponding to endosomes (N=4). (b) MDCK epithelial cells show longer lifetimes on the apical side (red on the side view) than on the basolateral part (green). The top view corresponds to a single confocal plane (between dashed lines in the left side view schematics), and depending on the height of the cells, either the apical side (red) or the basolateral part (green) are visible (N=4).

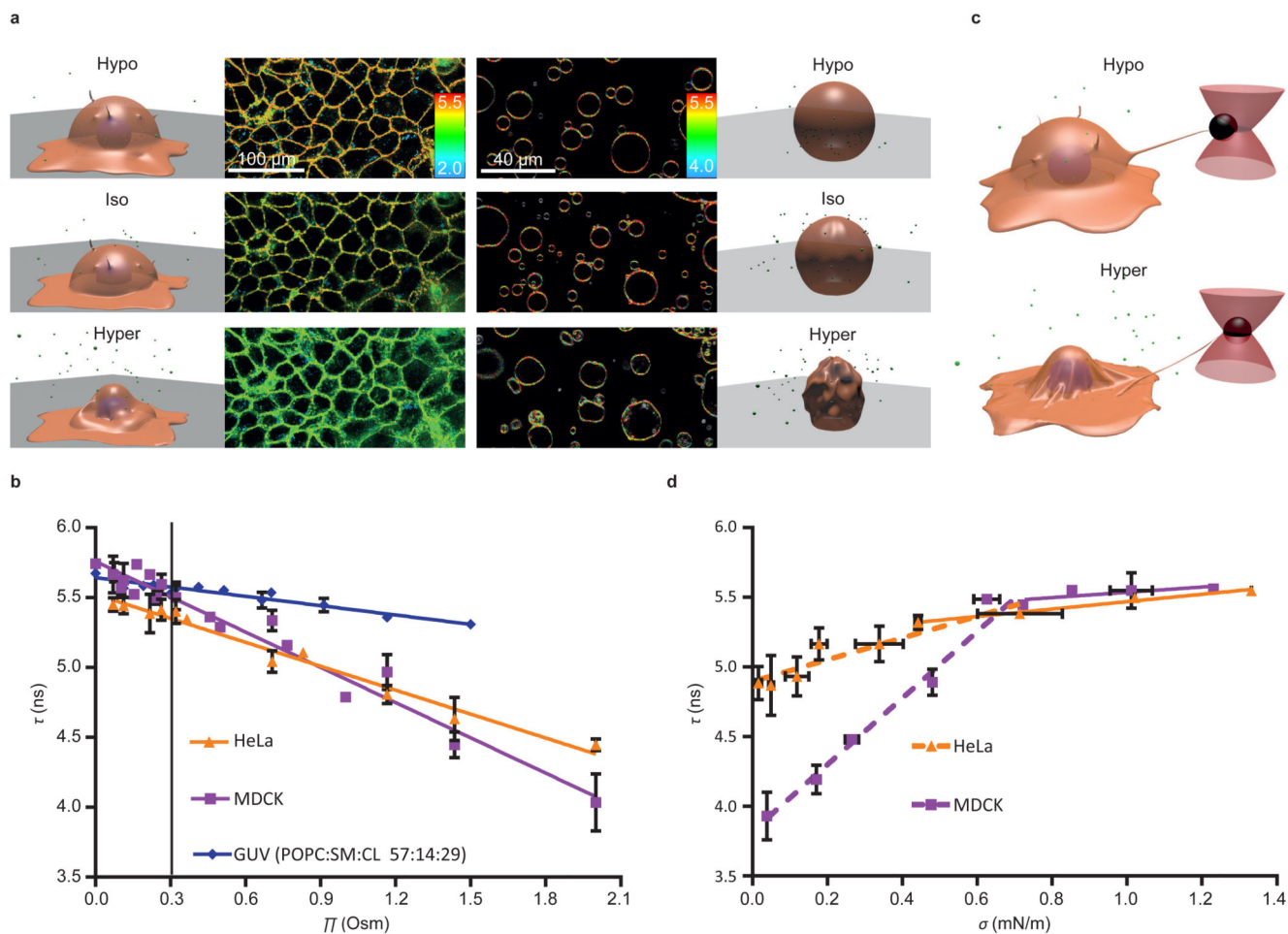


**Figure 3. Response of FliptR fluorescence lifetime to osmotic shocks on cells and GUVs.**

(a) FLIM images of MDCK and GUVs (POPC:SM:CL 57:14:29) in isoosmotic buffer, and after hyper- or hypoosmotic shocks. (b) FliptR fluorescence lifetime  $\tau_1$  as a function of the osmotic pressure  $\Pi$  applied to HeLa cells ( $\blacktriangle$ , slope hypo =  $-0.27 \pm 0.13$  ns·Osm $^{-1}$ , slope hyper =  $-0.59 \pm 0.04$  ns·Osm $^{-1}$ , Mean  $\pm$  SD as in the rest of the measurements, N=20), MDCK cells ( $\blacksquare$ , slope hypo =  $-0.50 \pm 0.33$  ns·Osm $^{-1}$ , slope hyper =  $-0.88 \pm 0.07$  ns·Osm $^{-1}$ , N=6) and GUVs ( $\blacklozenge$ , slope hypo =  $-0.19 \pm 0.18$  ns·Osm $^{-1}$ , slope hyper =  $-0.22 \pm 0.03$  ns·Osm $^{-1}$ , N=4), with linear curve fit, black line represents the initial state. (c) To correlate osmotic pressure  $\Pi$  with membrane tension  $\sigma$ , cells were connected to optical tweezers through pulled-out lipid nanotubes, and  $\sigma$  was calculated from the tube force measured in response to osmotic shocks applied. (d) FliptR fluorescence lifetime  $\tau_1$  as a function of the membrane tension  $\sigma$  applied by osmotic shocks to HeLa ( $\blacktriangle$ , slope hypo =  $0.26 \pm 0.06$  ns·m·mN $^{-1}$ , slope hyper =  $0.78 \pm 0.14$  ns·m·mN $^{-1}$ , N=7) and MDCK cells ( $\blacksquare$ , slope hypo =  $0.16 \pm 0.07$  ns·m·mN $^{-1}$ , slope hyper =  $2.38 \pm 0.18$  ns·m·mN $^{-1}$ , N=11) with pulled-out tubes connected to optical tweezers (c), with fit to the linear range before the onset of saturation above  $\tau_1 = 5.5$  ns).

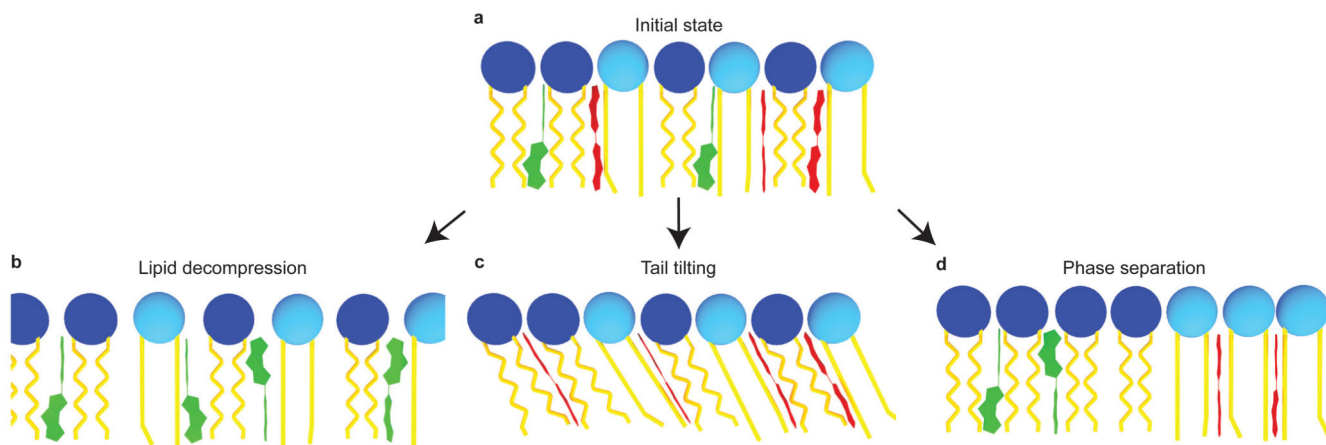


**Figure 4. Possible structural changes of lipid bilayer membranes in response to tension reported by FlptR.**

(a) Initial state where **FlptR** molecules are partially planarized in the membrane. Upon increasing tension, three structural changes could conceivably occur, namely (b) a loosening of the packing with increasing distance between less ordered lipid acyl chains, leading to **FlptR** deplanarization, (c) a tilting and stretching of more ordered acyl chains, which should lead to more compression of the **FlptR** probe and thus planarization, and (d) phase separation, in which case, **FlptR** molecules are more planarized in the  $L_0$  phase and less planarized in the  $L_d$  phase.

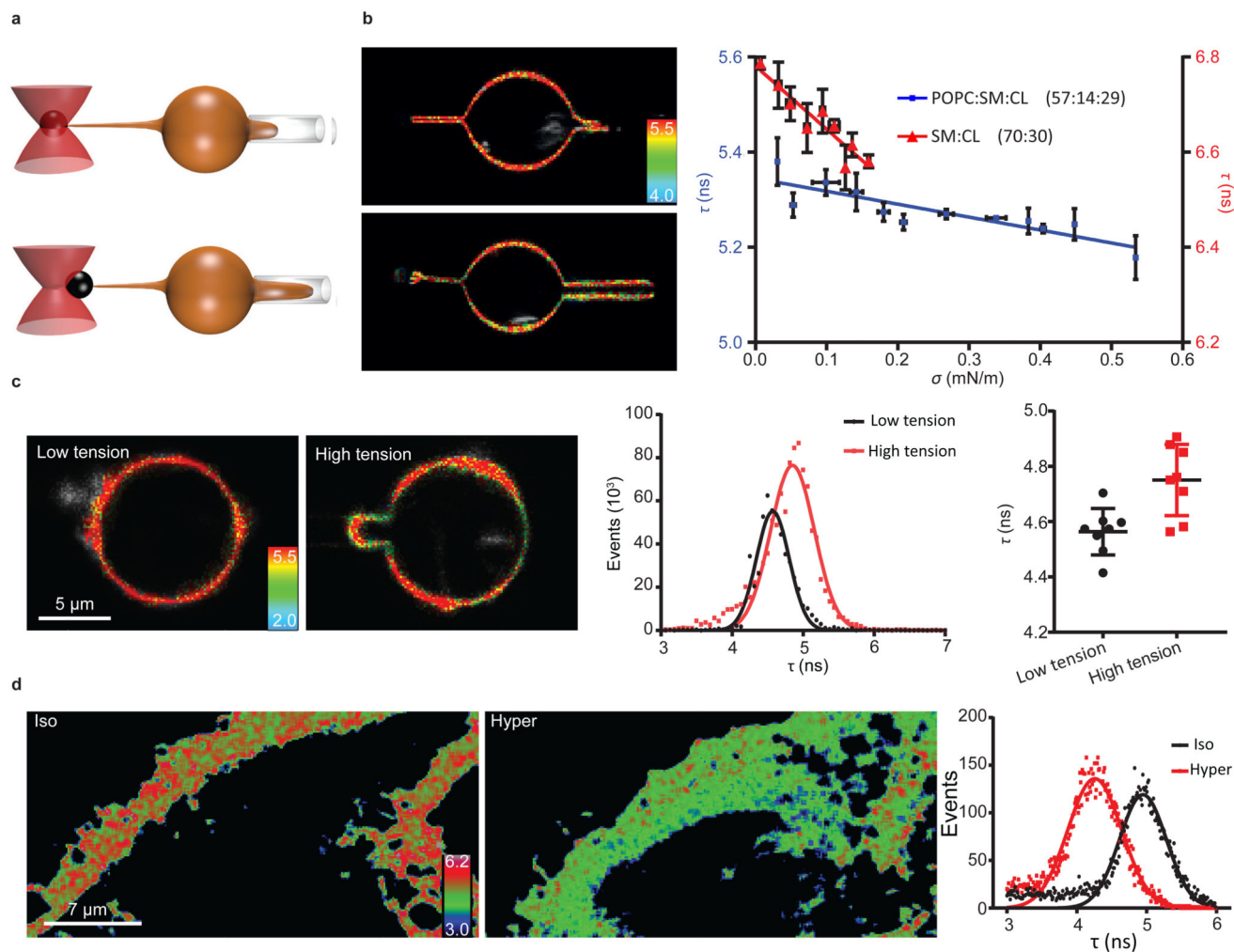


**Figure 5. Response of FLiPT lifetime to membrane tension in GUVs with and without phase separation induced by micropipette aspiration.**

(a) Schematics of the micropipette tube-pulling assay. (b) FLiM images and dependence of lifetimes  $\tau_1$  on membrane tension  $\sigma$  for SM/CL 70:30 ( $\blacktriangle$ , slope =  $-1.32 \pm 0.19$  ns·mN $^{-1}$ , N=6 GUVs) and POPC:SM:CL 57:14:29 ( $\blacksquare$ , slope =  $-0.27 \pm 0.05$  ns·mN $^{-1}$ , N=7 GUVs). (c) Left Panels: FLiM images of DOPC:SM:CL 30:30:40 GUVs aspirated in micropipettes and undergoing phase separation at high tension. Middle Panel: Distribution of the fluorescence lifetimes with Gaussian fits at low tension (Black) and high tension (red). Right panel: average lifetimes (N=8 GUVs) for GUVs at low tension (Black) and at high tension (Red) Error bars and the measure of center is the mean  $\pm$  SD. (d) Lifetime images of the membrane (confocal image of the lamellipodium) of a HeLa cell in isosmotic condition (Iso) and after hyperosmotic shock (Hyper), and the corresponding lifetime histograms (right panel) (N=3).

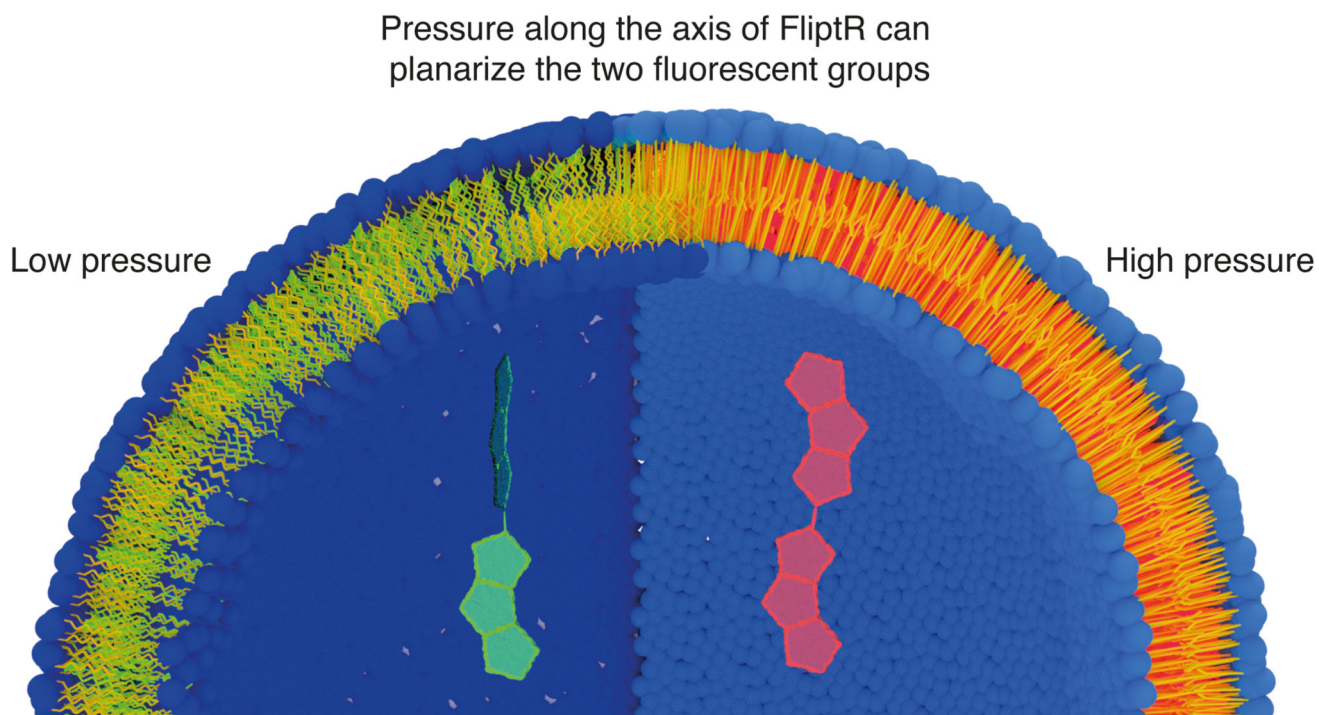


Figure 6.